Decomposition of Hydrogen Sulfide in Non-Thermal Plasma Aided by Supported $Zn_xCd_{1-x}S$ Solid Solutions

Y. Wang[1], L. Zhao[1], Z. Sun[1], X. Li[1], A. Wang[1], C. Song[1, 2], and Y. Hu[1]
[1]State Key Laboratory of Fine Chemicals, PSU-DUT Joint Center for Energy Research, School of Chemical Engineering, Dalian University of Technology, P.R. China
[2]EMS Energy Institute, Department of Energy and Mineral Engineering, the Pennsylvania State University, USA

Abstract—A series of $Zn_xCd_{1-x}S$ solid solutions supported on Al_2O_3 were prepared, and investigated in the plasma-induced H_2S decomposition. Structural and optical properties of the as-prepared catalysts were characterized by XRD, N_2 physisorption, UV-vis, TEM and XPS techniques. All $Zn_xCd_{1-x}S/Al_2O_3$ catalysts showed relatively high activities for H_2S decomposition. The catalytic activity is found to increase gradually when the Zn concentration on catalysts increases from 0.2 to 0.6. Subsequent increase in the Zn fraction up to 0.8 leads to lower H_2S conversion. Variation in activity is discussed in terms of modification in the conduction band and light absorption ability of $Zn_xCd_{1-x}S/Al_2O_3$ derived from the changes in the Zn/Cd molar ratio.

Keywords—Hydrogen sulfide, hydrogen, solid solution, non-thermal plasma

I. Introduction

Hydrogen sulfide (H_2S) is a highly toxic and corrosive contaminant in large quantities [1]. As a consequence, H_2S must be detoxified, in general, by the Claus process, in which H_2S is partially oxidized to produce elemental sulfur and water. On the other hand, H_2S has often been considered a potential source of hydrogen for the future hydrogen energy economy. Industrial hydrogen production by reforming consumes a large amount of fossil fuels and results in huge emissions of CO_2. Production of hydrogen by direct decomposition of H_2S may be an appealing approach to the hydrogen supply in the hydrotreating process in a refinery. The decomposition of H_2S, which produce hydrogen and elemental sulfur, needs less energy input to cleave the S-H bond than C-H bond in CH_4, O-H bond in H_2O, and N-H in NH_3, because S-H dissociation energy is the lowest. Nonetheless, the decomposition of H_2S is thermodynamically unfavorable, and limited by chemical equilibrium. Recently, we found that the combination of semiconductor catalysis with non-thermal plasma in a dielectric barrier discharge (DBD) reactor was extremely efficient to decompose H_2S for the production of hydrogen and sulfur at atmospheric pressure [2, 3]. When the decomposition of H_2S was performed in the DBD plasma with the aid of semiconductor catalysts (CdS/Al_2O_3 and ZnS/Al_2O_3), the conversion of H_2S increased dramatically. At relatively low energy consumption, 100% H_2S conversion was obtained. These results demonstrate a synergistic effect where both the plasma and catalyst are vital for the hydrogen production.

The key point of this technique is to synthesize semiconductor catalysts with high catalytic activity for H_2S decomposition. For efficient catalytic hydrogen production, a catalyst should meet two requirements, i.e., a high enough conduction band ensuring sufficient power for H_2S reduction to generate hydrogen and a narrow enough band gap allowing for maximum utilization of light [4, 5]. One of the strategies is the incorporation of ZnS into the structure of CdS to form $Zn_xCd_{1-x}S$ solid solutions [6-8]. The band gap of the solid solution can be continuously adjusted by changing its composition. As the Zn contents increases in the $Zn_xCd_{1-x}S$ solid solution, its conduction band would shift to more negative positions, which could lead to more efficient hydrogen generation than that of CdS [9, 10].

In this work, a series of $Zn_xCd_{1-x}S/Al_2O_3$ catalysts were prepared and resulted in high activity in the plasma-induced H_2S decomposition. The reason for their high activities was analyzed through XRD, N_2 physisorption, UV-vis, TEM and XPS characterizations.

II. Methodology

A. Catalyst Preparation

Al_2O_3 supported $Zn_xCd_{1-x}S$ solid solutions were used as catalysts. γ-Al_2O_3 extrudes (surface area: 270 m^2/g) were crushed and sieved to 40-60 mesh. The precursors of $Zn_xCd_{1-x}S/Al_2O_3$ with total loading of oxide precursor 10wt% were prepared by isometric impregnating Al_2O_3 with the mixture solution of $Cd(NO_3)_2$ and $Zn(NO_3)_2$ at room temperature. After the impregnation, the sample was dried at 120°C for 12 h, followed by calcination at 450°C for 5 h. And then the sample was sulfided in 10% H_2S/Ar flow (80 mL/min) for 3 h. The Al_2O_3 supported $Zn_xCd_{1-x}S$ solid solutions catalysts with different Zn/Cd molar ratio were prepared, marked as $Zn_xCd_{1-x}S/Al_2O_3$ (x = 0, 0.2, 0.4, 0.6, 0.8, and 1), respectively.

Corresponding author: Anjie Wang
e-mail address: ajwang@dlut.edu.cn

Presented at the 9th International Symposium on Non-Thermal/Thermal Plasma Pollution Control Technology & Sustainable Energy, in June 2014

B. Characterization

The XRD patterns of the samples were measured on a Rigaku D/Max 2400 diffractometer using nickel-filtered Cu Kα radiation at 40 kV and 100 mA. The BET surface areas of the catalysts were measured by N_2 adsorption at liquid N_2 temperature using a Micromeritic TriStarII 3020 instrument. UV-visible spectroscopy measurement was carried out on a Jasco V-550 spectrophotometer, using $BaSO_4$ as the reference sample. Transmission electron microscope (TEM) images of the samples were acquired on a JEM-2100 microscope operating at 200 kV. X-ray photoelectron spectra (XPS) were acquired with a Multilab-2000 X-ray photoelectron spectrometer, using an Al Kα source. All binding energies were referenced to the C 1s peak at 284.6 eV.

C. Catalystic Performance

The process of H_2S decomposition in a non-thermal plasma aided by semiconductor catalysts has been illustrated in detail in our previous study [2, 3]. The non-thermal plasma was generated at atmospheric pressure by dielectric barrier discharge (DBD). A high voltage generator (CTP-2000K; Corona Laboratory, Nanjing, China) was applied to supply a voltage (peak-to-peak voltage) from 0 to 15 kV with a sinusoidal waveform at a frequency of about 10 kHz. The DBD reactor mainly consists of a quartz tube and two electrodes (Fig. 1). The high-voltage electrode was a stainless-steel rod, which was installed along the axis of the quartz tube and connected to the generator. The grounding electrode was an aluminum foil, which was wrapped around the quartz tube and was connected to ground by a wire. Catalyst was placed into the gap between the quartz tube and the high-voltage electrode. The discharge power (the power applied to the reactor) was calculated using the Q-V Lissajous diagram, which was measured by a digital oscilloscope. The reactor was immersed in an oil bath, which was kept at 120°C to allow the generated sulfur to leave the catalyst bed in the form of liquid drops and to prevent sulfur deposition on the catalyst surface. A flow of feed gas (20vol% H_2S in Ar) was passed through the catalyst bed while a high voltage was applied to discharge the gas to form a non-thermal plasma. The effluent was passed through a saturated NaOH solution trap to remove unreacted H_2S, and the hydrogen content was analyzed by an on-line gas chromatograph equipped with a thermal conductivity detector. At 100% conversion, the effluent was rechecked with lead acetate test paper.

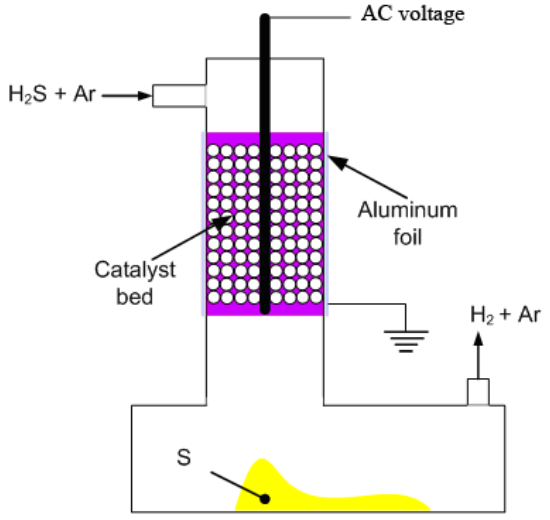

Fig. 1. Schematic diagram of the DBD reactor for semiconductor-catalyzed H_2S decomposition.

In H_2S decomposition, only H_2 and S are produced, without any other byproduct. Therefore, H_2S conversion (x_{H2S}) is equivalent to H_2 yield (Y_{H2}):

$$x_{H2S} = Y_{H2} = \frac{A_E}{A_0} \times 100\%$$

where A_E is the H_2 peak area in the chromatogram of the effluent, A_0 is the H_2 peak area at full H_2S conversion.

The area of the Lissajous diagram measures the energy dissipated in the discharge during one period of the voltage. The charge was determined by measuring the voltage across the capacitor of 0.47 μF connected in series to the ground line of the plasma reactor. The discharge power was calculated from the product of the area of charge-voltage parallelogram and the frequency of discharge (10 kHz). Specific input energy (SIE, J/L), which measures the energy input in the plasma process, was calculated by:

$$SIE = \frac{P}{V}$$

where P is the discharge power (W), and V is the gas flow rate (L/s).

The energy consumption for hydrogen production (E, eV) was calculated from SIE, H_2 yield and initial H_2S concentration (20%):

$$E = \frac{SIE}{Y_{H2} \cdot 20\%} \times \frac{22.4}{96}$$

III. Results and Discussion

A. XRD Analysis

Fig. 2 shows XRD patterns of CdS/Al_2O_3, ZnS/Al_2O_3 and $Zn_xCd_{1-x}S/Al_2O_3$ for various x values. The characteristic diffraction peaks for CdS/Al_2O_3 were observed at 2θ of 24.8°, 26.5°, 28.2°, 43.7°, 47.9° and 51.9° and were attributed to the (1 0 0), (0 0 2), (1 0 1), (1 1 0), (1 0 3), and (1 1 2) crystal planes of CdS, which was indexed to hexagonal CdS (JCPDS#06-0314). Similarly, ZnS/Al_2O_3 was found to exhibit three peaks located at 2θ of 28.6°, 47.6° and 56.5°, which originated from the (1 1 1), (2 2 0) and (3 1 1) crystal planes of cubic zincblende ZnS (JCPDS#65-0309). Moreover, the

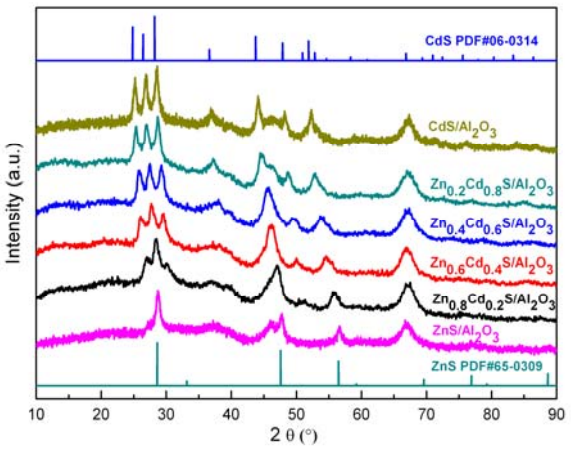

Fig. 2. XRD patterns of ZnS/Al_2O_3, CdS/Al_2O_3 and $Zn_xCd_{1-x}S/Al_2O_3$ (x = 0.2, 0.4, 0.6 and 0.8) catalysts.

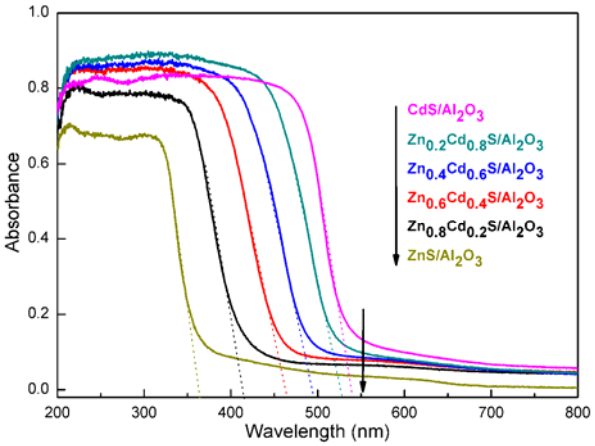

Fig. 3. UV-vis diffuse reflection spectra for ZnS/Al_2O_3, CdS/Al_2O_3 and $Zn_xCd_{1-x}S/Al_2O_3$ (x = 0.2, 0.4, 0.6 and 0.8) catalysts.

TABLE I
BET SURFACE AREA, PARTICLE SIZE AND BAND GAP OF THE CATALYSTS

Catalyst	BET surface area (m^2/g)	Particle size (nm)	Band gap (eV)
CdS/Al_2O_3	205	10.7	2.29
$Zn_{0.2}Cd_{0.8}S/Al_2O_3$	222	9.4	2.36
$Zn_{0.4}Cd_{0.6}S/Al_2O_3$	221	8.3	2.50
$Zn_{0.6}Cd_{0.4}S/Al_2O_3$	220	8.1	2.67
$Zn_{0.8}Cd_{0.2}S/Al_2O_3$	226	8.9	2.97
ZnS/Al_2O_3	213	10.0	3.40

diffraction peaks of the $Zn_xCd_{1-x}S/Al_2O_3$ catalysts shifted to higher angles upon increasing x value. The successive shifts in the XRD patterns indicated that the crystals obtained were attributable of $Zn_xCd_{1-x}S$ solid solutions. It is considered that the Zn^{2+} incorporated in the CdS lattice or entered its interstitial sites because the radius of Zn^{2+} ion (0.74 Å) is smaller than that of Cd^{2+} (0.97 Å) [10]. Additionally, the gradual up-shift of XRD peak positions of the $Zn_xCd_{1-x}S/Al_2O_3$ with the increasing of Zn/Cd molar ratio from CdS to ZnS, together with no additional diffraction peaks corresponding to CdS and ZnS, suggests that the crystals obtained were not a mixture of CdS and ZnS but $Zn_xCd_{1-x}S$ solid solution [11].

As shown in Table I, BET surface areas of $Zn_xCd_{1-x}S/Al_2O_3$ catalysts were measured to be around 220 m^2/g, and the variations of the average size calculated from the Scherrer formula were also calculated. The crystal sizes of the solid solution were estimated to be 10.7, 9.4, 8.3, 8.1, 8.9, and 10.0 nm for the $Zn_xCd_{1-x}S/Al_2O_3$ catalysts of which x value was 0, 0.2, 0.4, 0.6, 0.8 and 1, respectively. As it is observed, the average particle size of solid solution crystalline domains decreases gradually when the Zn concentration raises up to 0.6 increasing subsequently. The observed variations in particle size were mainly associated to the presence of Zn in the CdS crystals. As pointed by Anpo *et al.* [12], small nanoparticles with poor crystallinity favor the migration of generated charges from bulk to the surface over short distance, which is regarded as a key factor for the acceleration of photocatalytic activity. Moreover, smaller particles inevitably increase the active phase dispersion and provide more reactive sites for the reactants than aggregated particles.

B. UV-vis Analysis

Fig. 3 shows the diffuse reflectance UV-vis absorption spectra of the various solid solutions catalysts of $Zn_xCd_{1-x}S/Al_2O_3$, as well as ZnS/Al_2O_3 and CdS/Al_2O_3. The absorption onsets were determined by liner extrapolation from the inflection point of the curve to the baseline. ZnS/Al_2O_3 had an absorption edge located about 365 nm, whereas the absorption edges of $Zn_xCd_{1-x}S/Al_2O_3$ solid solutions were gradually red shifted as the Zn content (x value) decreases from 0.80 to 0.20. Continuous shift of the absorption edges indicates that the band gap of the solid solution catalyst can be precisely controlled with the variation of Zn/Cd molar ratio. Furthermore, intense absorption bands with steep absorption edges were observed for all the spectra, indicating that the light absorption was contributed by the intrinsic band gap transition rather than the transition from impurity levels [6]. The results of XRD patterns and UV-vis spectra both provide evidence that the homogeneous $Zn_xCd_{1-x}S$ solid solution were formed.

The relationship of the absorption coefficient and the incident photon energy of semiconductor can be estimated by the Kubelka-Munk equation [13]:

$$\alpha(h\nu)=C(h\nu- Eg)^{n/2}$$

where α is the absorption coefficient and its value can be obtained by the equation: $\alpha = (1-R)^2/2R$, R is the diffuse reflectance and its relationship with absorbance can be defined by $R = 10^{-A}$, A is absorbance. h is Planck's constant, ν is frequency, and C is a constant. For a direct transition semiconductor, n = 1; for an indirect transition semiconductor, n = 4. The nature of transition is possible to be determined through plotting the graph of $(\alpha h\nu)^2$ versus hν, thereby the band gap energies can be deduced by extrapolating the straight-linear portions of the plot to

intersect the photon energy axis. As shown in Table I, the band gaps obtained in such a way were approximately 2.29, 2.36, 2.50, 2.67, 2.97 and 3.40 eV for the $Zn_xCd_{1-x}S/Al_2O_3$ (x = 0, 0.2, 0.4, 0.6, 0.8 and 1.0), respectively. For all the $Zn_xCd_{1-x}S/Al_2O_3$ catalysts, a monotonic increase of the band gap is observed with the increase of the Zn-content in the $Zn_xCd_{1-x}S$ solid solution. Therefore, the band gap position of the $Zn_xCd_{1-x}S$ solid solutions could be adjusted by changing the Zn/Cd molar ratio. Compositional variation of $Zn_xCd_{1-x}S$ solid solutions affect their band gap because the replacement of Cd cations by Zn in the crystal lattice modifies the position of the conduction band by the hybridization of the Cd 5s5p level with the more negative Zn 4s4p level [14]. The band gap modulation observed was also thought to be capable of effectively changing the relative redox ability of solid solutions catalysts [9].

C. TEM Analysis

Fig. 4 reveals the morphology and microstructure of the solid solutions by taking the composition of $Zn_{0.6}Cd_{0.4}S/Al_2O_3$ as a typical sample. The interplanar spacing was about 3.274 Å, which is in good agreement with the interplanar distance of the (1 1 1) plane of $Zn_{0.6}Cd_{0.4}S$ (3.271 Å). In accordance with the peak-shift in the XRD patterns, the value of the (1 1 1) of $Zn_{0.6}Cd_{0.4}S$ is bigger than that of ZnS (3.118 Å), which can be explained due to the higher radius of Cd^{2+} than that of Zn^{2+}. In addition, the TEM image also indicates that the average diameter of nanoparticles was about 6-10 nm. The result matched well with the particle size estimated from the Scherrer equation.

D. XPS Analysis

The XPS technique has been used to examine the chemical state of the elements and their surface proportion in the ZnS/Al_2O_3, CdS/Al_2O_3 and $Zn_xCd_{1-x}S/Al_2O_3$ catalysts. Fig. 5 (a) and (b) displays the Cd 3d and Zn 2p spectra of catalysts, respectively. For CdS/Al_2O_3 catalyst, the observed binding energy of Cd (3d5/2) was 405.5 eV, which agrees with values reported for Cd^{2+} in sulphides [15, 16]. The binding energy of Zn 2p3/2 peak at about 1022.1 eV in ZnS/Al_2O_3 catalyst was characteristic of Zn^{2+} ions in an environment of S^{2-} species [17]. The $Zn_xCd_{1-x}S/Al_2O_3$ catalysts exhibited a progressive increase in the binding energy of Cd 3d5/2 with the increase of Zn concentration in the catalysts formulation (from 405.5 eV observed for CdS/Al_2O_3 to 405.9 eV observed for the $Zn_{0.8}Cd_{0.2}S/Al_2O_3$ catalyst). A similar situation can also be observed in the case of Zn 2p peaks that were shifted to higher values of binding energies with the increase of Zn/Cd molar ratio. The observed changes in the binding energies of Cd 3d and

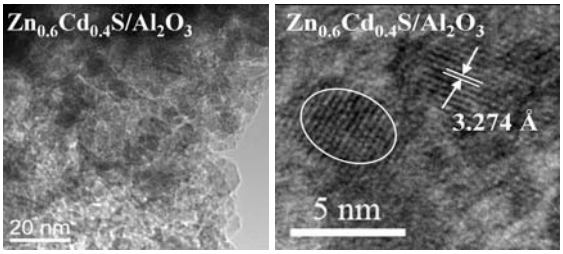

Fig. 4. TEM images of $Zn_{0.6}Cd_{0.4}S/Al_2O_3$ catalyst.

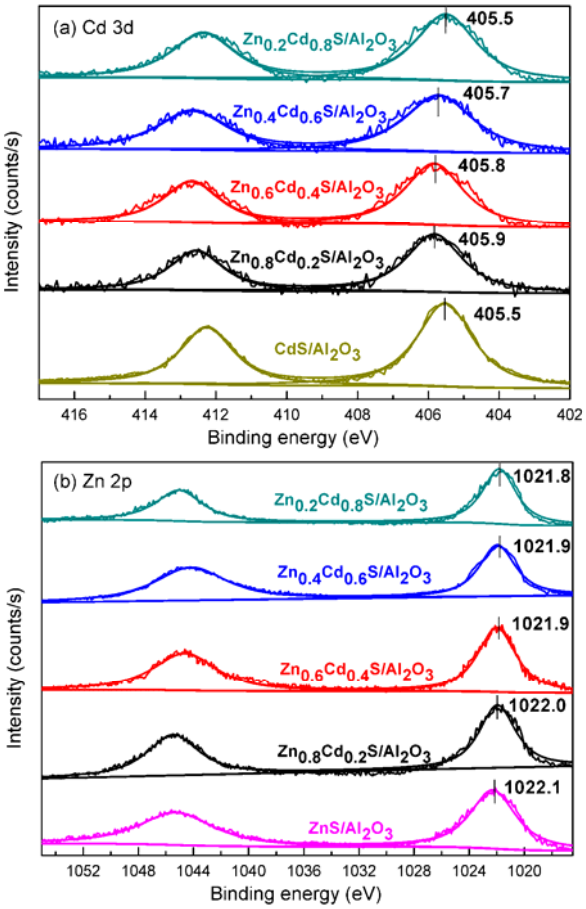

Fig. 5. XPS spectra of $Zn_xCd_{1-x}S/Al_2O_3$ (x = 0.2, 0.4, 0.6 and 0.8) catalysts. (a) XPS spectrum of Cd 3d; (b) XPS spectrum of Zn 2p.

TABLE II
SURFACE COMPOSITION OF $Zn_xCd_{1-x}S/Al_2O_3$ (x = 0.2, 0.4, 0.6 and 0.8) CATALYSTS

Catalyst	Surface compositions (mol%)						
	Zn	Cd	S	O	Al	Zn/Cd	S/(Cd+Zn)
$Zn_{0.2}Cd_{0.8}S/Al_2O_3$	0.42	1.53	1.96	63.08	33.01	0.27	1.01
$Zn_{0.4}Cd_{0.6}S/Al_2O_3$	0.69	0.92	1.62	61.34	35.43	0.75	1.01
$Zn_{0.6}Cd_{0.4}S/Al_2O_3$	0.80	0.59	1.52	63.86	33.23	1.36	1.09
$Zn_{0.8}Cd_{0.2}S/Al_2O_3$	1.16	0.21	1.38	63.52	33.73	5.52	1.01

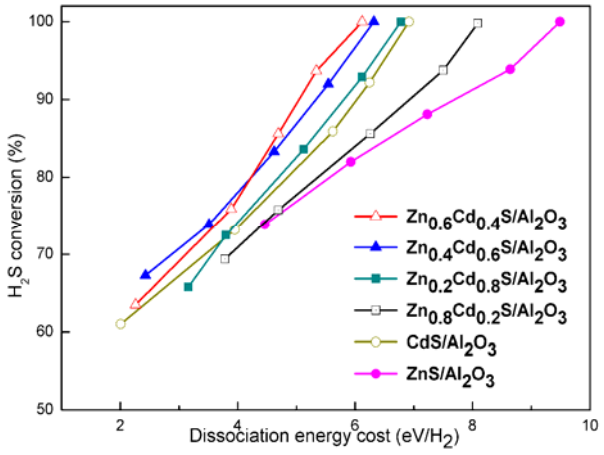

Fig. 6. H_2S conversion as a function of dissociation energy cost in the plasma-induced decomposition over $Zn_xCd_{1-x}S/Al_2O_3$, CdS/Al_2O_3 and ZnS/Al_2O_3 catalysts. Reaction conditions: catalyst bed volume: 15 mL; feed: 20% H_2S in Ar; GHSV: 120 h^{-1}.

Zn 2p with Zn/Cd molar ratio may be related to the formation $Zn_xCd_{1-x}S$ solid solutions in which Zn and Cd interact, and some transfer of electrons takes place from Cd to Zn atoms in the lattice [18].

Surface concentrations of Cd, Zn, S, O and Al calculated from XPS intensities are listed in Table II. As expected, the surface exposure of zinc species increases with an increase in the Zn loading of catalysts, however, the Zn/Cd molar ratio is somewhat higher than the nominal value, indicating that the surface of $Zn_xCd_{1-x}S$ nanoparticles becomes slightly Zn-enriched. Moreover, it can be seen that the S/(Cd + Zn) atom ratio was close to unity suggesting that the sulfidation degree was almost complete.

E. Catalytic Decomposition of Hydrogen Sulfide

As Fig. 6 shows, the catalytic activities were found to increase gradually when the Zn concentration on catalysts increased from 0.2 to 0.6. Subsequent increased in the Zn concentration up to 0.8 led to lower H_2S conversion. Furthermore, it can be clearly observed that all of the $Zn_xCd_{1-x}S/Al_2O_3$ solid solutions catalysts exhibit better activities of H_2S decomposition than that of ZnS/Al_2O_3. Among them, $Zn_{0.6}Cd_{0.4}S/Al_2O_3$ and $Zn_{0.4}Cd_{0.6}S/Al_2O_3$ catalysts showed higher catalytic activity than CdS/Al_2O_3. At an energy consumption of 6.12 eV/H_2, H_2S conversions were 100%, 97.9%, 92.8%, 90.9%, 84.9% and 82.9%, when $Zn_{0.6}Cd_{0.4}S/Al_2O_3$, $Zn_{0.4}Cd_{0.6}S/Al_2O_3$, $Zn_{0.2}Cd_{0.8}S/Al_2O_3$, CdS/Al_2O_3, $Zn_{0.8}Cd_{0.2}S/Al_2O_3$ and ZnS/Al_2O_3 were filled in the gap, respectively.

The photophysical properties, as light absorption and position of conduction and valence bands, are associated to semiconductor catalyst composition. High catalytic activities are associated to high light absorption with a conduction band level higher than reduction H^+/H_2 potential and a low h^+/e^- recombination. Although the addition of the higher band gap semiconductor ZnS is disadvantageous to light absorption, it elevates the conduction band position of the catalyst, which is very important to the enhancement of the hydrogen production [9-11, 14]. Therefore, there is a delicate balance between the light absorption and the level of conduction band of $Zn_xCd_{1-x}S$ solid solutions that is necessary to be kept. What is more, Xing *et al.* [19] also proposed that an appropriate amount of doping-Zn into the lattice or interstitial of CdS provided suitable impurity energy levels which made the excited electrons from the valence band of CdS easily inject into the conduction band.

The characterizations of $Zn_xCd_{1-x}S/Al_2O_3$ prepared in this study show that the variation in Zn/Cd molar ratio induces significant structural and photooptical changes on the catalysts. As shown in Table I, particle size of solid solutions decreased gradually with Zn up to 0.6, increasing subsequently when the Zn concentration exceeded 0.8. The small particle size would facilitate faster transportation of electrons from bulk to surface avoiding their recombination in the bulk of the catalyst [12, 20]. Therefore, the decrease in particle size of the $Zn_xCd_{1-x}S$ solid solutions also contributes to the higher activity. Meanwhile, $Zn_xCd_{1-x}S/Al_2O_3$ possesses a higher BET surface area (Table I). The higher BET surface area is beneficial to absorb more light, and will increase the effective reaction sites as well as shorten the diffuse distances of the photogenerated carriers [19, 21]. Moreover, the changes in Zn/Cd molar ratios of catalysts have effect on their photophysical properties with a monotonous variation in band gap size with the increase in the Zn atomic fraction (Table I). The continuous shift in band gap energy with Zn content agrees well with the trend expected for similar sulfide solid solutions in which the change in band gap energy is associated to an increase in the position of the conduction band by the hybridization of Cd 5s5p level with the more negative Zn 4s4p level [22]. Additionally, according to Zhang *et al.* [23], the $Zn_xCd_{1-x}S$ solid solutions prepared by a thermal sulfuration process could improve catalytic activity due to the uneven distribution of anionic S^{2-} ions. The existence of this charge gradient may promote the charge separation of h^+/e^- pairs and avoid their recombination in the bulk semiconductor, thus leading to significantly improved catalytic hydrogen production.

$Zn_{0.6}Cd_{0.4}S/Al_2O_3$ exhibited higher performance than other catalysts, achieving full conversion at lower energy cost. However, as shown in Fig. 6, when the Zn fraction was raised from 0.4 to 0.6, the increase in activity was moderate and this in spite of the decrease in particle size and the increase in energy level of the conduction band achieved in $Zn_{0.6}Cd_{0.4}S/Al_2O_3$ catalyst. Furthermore, at low energy input, $Zn_{0.4}Cd_{0.6}S/Al_2O_3$ showed higher catalytic activity than $Zn_{0.6}Cd_{0.4}S/Al_2O_3$ catalyst. The explanation for these experimental results may be related with the counteracting effect of the decrease of h^+/e^- pair population associated to the increase in the band gap of the catalyst. Electrons in a larger band gap catalyst require more energy to jump to the conduction band (CB) from the valence band (VB). In non-thermal plasma, the intensity of electric field and light is dependent on energy input. Higher energy input, higher intensity of electric

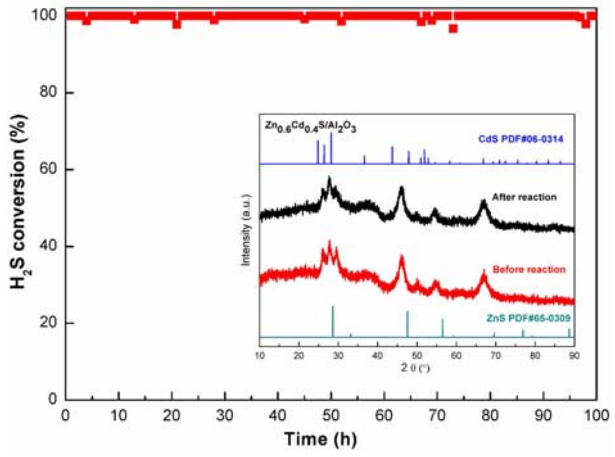

Fig. 7. H_2S conversion with time in the plasma-induced decomposition over $Zn_{0.6}Cd_{0.4}S/Al_2O_3$. Reaction conditions: SIE: 6.0 kJ/L; catalyst bed volume: 15 mL; feed: 20% H_2S in Ar; GHSV: 120 h^{-1}.

field and light. As a result, the h^+/e^- pair population on larger band gap catalyst ($Zn_{0.6}Cd_{0.4}S/Al_2O_3$) is lower at low energy input due to the low light intensity and electric field intensity. However, the intensity of electric field and light increases with energy input. Moreover, with the increasing of Zn/Cd ratio, the solid solutions have worse photoabsorption but better redox ability. As a balance of the two main effects, the more negative potential of the conduction band of $Zn_{0.6}Cd_{0.4}S/Al_2O_3$ allows for more efficient hydrogen generation at high energy input.

The H_2S conversion variation in H_2S decomposition over $Zn_{0.6}Cd_{0.4}S/Al_2O_3$ in the long-term test is presented in Fig. 7. The stability of catalyst at full conversion was investigated. The result demonstrated that catalyst was stable in the 100 h test runs. The XRD patterns of $Zn_{0.6}Cd_{0.4}S/Al_2O_3$ before and after the reaction hardly changed, suggesting that the crystal structure of $Zn_{0.6}Cd_{0.4}S/Al_2O_3$ underwent no change in the H_2S plasma.

IV. Conclusion

The control of the energy structure of CdS/Al_2O_3 by making solid solutions with ZnS ($Zn_xCd_{1-x}S/Al_2O_3$ $x = 0.2$-0.8) was investigated for its application in H_2S decomposition in non-thermal plasma. All $Zn_xCd_{1-x}S/Al_2O_3$ catalysts showed relatively high activities for H_2S decomposition. With the adding of ZnS, the solid solutions have worse photoabsorption but better redox ability. As a balance of the two main effects, $Zn_{0.6}Cd_{0.4}S/Al_2O_3$ and $Zn_{0.4}Cd_{0.6}S/Al_2O_3$ exhibited higher performance than CdS/Al_2O_3 and ZnS/Al_2O_3, achieving full conversion at lower energy cost.

Acknowledgment

The authors acknowledge the financial supports from NSFC (20773020, 20973030, 21173033, U1162203), the "863" Project (2008AA030803), and the Ph.D. Programs of MOE (20100041110016).

References

[1] R. G. Hendrickson, A. Chang, and R. J. Hamilton, "Co-worker fatalities from hydrogen sulfide," *American Journal of Industrial Medicine*, vol. 45, pp. 346-350, 2004.

[2] L. Zhao, Y. Wang, L. Jin, M. L. Qin, X. Li, A. J. Wang, C. S. Song, and Y. K. Hu, "Decomposition of hydrogen sulfide in non-thermal plasma aided by supported CdS and ZnS semiconductors," *Green Chemistry*, vol. 15, pp. 1509-1513, 2013.

[3] L. Zhao, Y. Wang, X. Li, A. J. Wang, C. S. Song, and Y. K. Hu, "Hydrogen production via decomposition of hydrogen sulfide by synergy of non-thermal plasma and semiconductor catalysis," *International Journal of Hydrogen Energy*, vol. 38, pp. 14415-14423, 2013.

[4] A. Kudo, H. Kato, and I. Tsuji, "Strategies for the development of visible-light-driven photocatalysts for water splitting," *Chemistry Letters*, vol. 33, pp. 1534-1539, 2004.

[5] X. H. Zhang, D. W. Jing, M. C. Liu, and L. J. Guo, "Efficient photocatalytic H_2 production under visible light irradiation over Ni doped $Cd_{1-x}Zn_xS$ microsphere photocatalysts," *Catalysis Communications*, vol. 9, pp. 1720-1724, 2008.

[6] L. Wang, W. Z. Wang, M. Shang, W. Z. Yin, S. M. Sun, and L. Zhang, "Enhanced photocatalytic hydrogen evolution under visible light over $Cd_{1-x}Zn_xS$ solid solution with cubic zinc blend phase," *International Journal of Hydrogen Energy*, vol. 35, pp. 19-25, 2010.

[7] X. Xu, R. J. Lu, X. F. Zhao, S. L. Xu, X. D. Lei, F. Z. Zhang, and D. G. Evans, "Fabrication and photocatalytic performance of a $Zn_xCd_{1-x}S$ solid solution prepared by sulfuration of a single layered double hydroxide precursor," *Applied Catalysis B-Environmental*, vol. 102, pp. 147-156, 2011.

[8] Y. Q. Chen, X. H. Zhang, C. Jia, Y. Su, and Q. Li, "Synthesis and Characterization of ZnS, CdS, and Composition-Tunable ZnxCd1-xS Alloyed Nanocrystals via a Mix-Solvothermal Route," *Journal of Physical Chemistry C*, vol. 113, pp. 2263-2266, 2009.

[9] L. X. Song, H. W. Wei, H. Xu, and J. H. Zhan, "Ethanol-thermal synthesis of $Cd_{1-x}Zn_xS$ nanoparticles with enhanced photodegradation of 4-chlorophenol," *Materials Research Bulletin*, vol. 45, pp. 1396-1400, 2010.

[10] M. T. Li, J. G. Jiang, and L. J. Guo, "Synthesis, characterization, and photoelectrochemical study of $Cd_{1-x}Zn_xS$ solid solution thin films deposited by spray pyrolysis for water splitting," *International Journal of Hydrogen Energy*, vol. 35, pp. 7036-7042, 2010.

[11] X. H. Zhong, Y. Y. Feng, W. Knoll, and M. Y. Han, "Alloyed $Zn_xCd_{1-x}S$ nanocrystals with highly narrow luminescence spectral width," *Journal of the American Chemical Society*, vol. 125, pp. 13559-13563, 2003.

[12] M. Anpo, T. Shima, S. Kodama, and Y. Kubokawa, "Photocatalytic hydrogenation of propyne with water on small-particle titania: size quantization effects and reaction intermediates," *The Journal of Physical Chemistry*, vol. 91, pp. 4305-4310, 1987.

[13] K. Domen, A. Kudo, and T. Onishi, "Mechanism of photocatalytic decomposition of water into H_2 and O_2 over NiO-$SrTiO_3$," *Journal of Catalysis*, vol. 102, pp. 92-98, 1986.

[14] D. V. Petrov, B. S. Santos, G. A. L. Pereira, and C. D. Donega, "Size and band-gap dependences of the first hyperpolarizability of $Cd_xZn_{1-x}S$ nanocrystals," *Journal of Physical Chemistry B*, vol. 106, pp. 5325-5334, 2002.

[15] S. Celebi, A. K. Erdamar, A. Sennaroglu, A. Kurt, and H. Y. Acar, "Synthesis and characterization of poly(acrylic acid) stabilized cadmium sulfide quantum dots," *Journal of Physical Chemistry B*, vol. 111, pp. 12668-12675, 2007.

[16] A. Deshpande, P. Shah, R. S. Gholap, and N. M. Gupta, "Interfacial and physico-chemical properties of polymer-supported CdS center dot ZnS nanocomposites and their role in the visible-light mediated photocatalytic splitting of water," *Journal of Colloid and Interface Science*, vol. 333, pp. 263-268, 2009.

[17] J. D. G. Duran, M. C. Guindo, A. V. Delgado, and F. GonzalezCaballero, "Surface chemical analysis and electrokinetic properties of synthetic spherical mixed zinc-cadmium sulfides," *Journal of Colloid and Interface Science*, vol. 193, pp. 223-233, 1997.

[18] W. Zhang and R. Xu, "Surface engineered active photocatalysts without noble metals: CuS-$Zn_xCd_{1-x}S$ nanospheres by one-step synthesis," *International Journal of Hydrogen Energy*, vol. 34, pp. 8495-8503, 2009.

[19] C. J. Xing, Y. J. Zhang, W. Yan, and L. J. Guo, "Band structure-controlled solid solution of $Cd_{1-x}Zn_xS$ photocatalyst for hydrogen production by water splitting," *International Journal of Hydrogen Energy*, vol. 31, pp. 2018-2024, 2006.

[20] N. Z. Bao, L. M. Shen, T. Takata, and K. Domen, "Self-templated synthesis of nanoporous CdS nanostructures for highly efficient photocatalytic hydrogen production under visible," *Chemistry of Materials*, vol. 20, pp. 110-117, 2008.

[21] J. S. Hu, L. L. Ren, Y. G. Guo, H. P. Liang, A. M. Cao, L. J. Wan, and C. L. Bai, "Mass production and high photocatalytic activity of ZnS nanoporous nanoparticles," *Angewandte Chemie-International Edition*, vol. 44, pp. 1269-1273, 2005.

[22] I. Tsuji, H. Kato, H. Kobayashi, and A. Kudo, "Photocatalytic H_2 evolution reaction from aqueous solutions over band structure-controlled $(AgIn)_xZn_{2(1-x)}S_2$ solid solution photocatalysts with visible-light response and their surface nanostructures," *Journal of the American Chemical Society*, vol. 126, pp. 13406-13413, 2004.

[23] K. Zhang, D. W. Jing, C. J. Xing, and L. J. Guo, "Significantly improved photocatalytic hydrogen production activity over $Cd_{1-x}Zn_xS$ photocatalysts prepared by a novel thermal sulfuration method," *International Journal of Hydrogen Energy*, vol. 32, pp. 4685-4691, 2007.